Journal of Alloys and Compounds 509 (2011) 2850–2855

Contents lists available at ScienceDirect

Journal of Alloys and Compounds

journal homepage: www.elsevier.com/locate/jallcom

Photoluminescence properties and energy-transfer of thermal-stable Ce^{3+}, Mn^{2+}-codoped barium strontium lithium silicate red phosphors

Xinguo Zhang, Menglian Gong*

Ministry of Education Laboratory of Bioinorganic and Synthetic Chemistry, State Key Laboratory of Optoelectronic Materials and Technologies, School of Chemistry and Chemical Engineering, Sun Yat-sen University, XIngang Xi Road 135, Guangzhou 510275, China

ARTICLE INFO

Article history:
Received 22 July 2010
Received in revised form
23 November 2010
Accepted 23 November 2010
Available online 1 December 2010

Keywords:
BSLS:Ce^{3+}, Mn^{2+}
Photoluminescence
Energy transfer

ABSTRACT

A series of thermal-stable Ce^{3+}, Mn^{2+}-codoped barium strontium lithium silicate (BSLS) phosphors was synthesized by a high-temperature solid-state reaction. The XRD patterns of this phosphor seem to be a new phase that has not been reported before. BSLS:Ce^{3+}, Mn^{2+} showed two emission bands under 365 nm excitation: one observed at 421 nm was attributed to Ce^{3+} emission, and the other found in red region was assigned to Mn^{2+} emission through Ce^{3+}–Mn^{2+} efficient energy transfer. The Mn^{2+} emission shifted red along with the replacement of barium by strontium, which was due to the change of crystal field. A composition-optimized phosphor, BSLS:0.10Ce^{3+}, 0.05Mn^{2+} (Ba = 65), exhibited strong and broad red-emitting and supreme thermal stability. The results suggest that this phosphor is suitable as a red component for NUV LED or high pressure Hg vapor (HPMV) lamp.

1. Introduction

Recently, commercial phosphor converted (pc-) WLEDs made by means of blue-LED plus YAG:Ce yellow phosphors suffer some weaknesses, such as poor color rendering index and low stability of color temperature [1]. White UV-LEDs fabricated by UV-LED chips coated with red–green–blue tri-color phosphors could conquer the afore-mentioned problems owing to the invisible emission of the LED chip and white color generated by phosphors [2]. The blue and green phosphors, such as $Ca_5(PO_4)_3Cl$:Eu^{2+}, $BaMgAl_{14}O_{23}$:Eu^{2+}/Mn^{2+}, $BaMgAl_{10}O_{17}$:Eu^{2+}/Mn^{2+}, etc. are commercially available and could meet the requirements of NUV excitation in terms of spectra [3]. However, the identified red phosphors for NUV white LED application are scarce. The excitation efficiency of the existing red-emitting phosphors such as YVO_4:Eu^{3+} and Y_2O_2S:Eu^{3+} declines dramatically in the NUV region. Besides, the emission of Eu^{3+} is sharp lines, which is not favorable to generate white light with high luminous efficiency and good color rendering index [4]. Therefore, exploring new red phosphors is a prerequisite for NUV-LED applications.

Mn^{2+} ion exhibits broad-band red emission due to its $^4T_1 \rightarrow {}^6A_1$ transition in a suitable host [5]. However, it has a weak emission because its *d–d* absorption transition is spin forbidden when Mn^{2+} is solely doped [6,7]. In general, the method to enhance the emission intensity of Mn^{2+} is by introducing sensitizer Eu^{2+}/Ce^{3+} because of its high efficiency for both excitation and emission in many hosts, like $Ba_3MgSi_2O_8$ [8], $BaMg_2Si_2O_7$ [9,10] and $MgSiO_3$ [11]. Typically, Eu^{2+}/Ce^{3+} can transfer its absorbed energy fully or partly to Mn^{2+}, consequently orange-reddish [12,13] or single-phase-full-color [14,15] phosphors can be obtained. Hence, Eu^{2+}/Ce^{3+} and Mn^{2+} co-doped luminescent materials have been studied extensively over the past few years [16–18]. For instance, Chen and co-workers firstly synthesized the tunable blue–white–red $Ca_{10}K(PO_4)_7$:Eu^{2+}, Mn^{2+} phosphor and investigated the energy transfer mechanism [19]. Later, they further reported the red-emitting $Ca_9Y(PO_4)_7$:Ce^{3+}, Mn^{2+} phosphor for fluorescent lamp application [20].

In recent years, the luminescent properties of silicate materials have been widely investigated because of the advantages such as excellent thermal and chemical stability [21,22]. Especially, many Eu^{2+}/Ce^{3+} and Mn^{2+} co-doped silicate red phosphors have been studied, such as $Ba_3MgSi_2O_8$:Eu^{2+}, Mn^{2+} [23], $MgYSi_2O_5N$:Ce^{3+}, Mn^{2+} [24], $CaSiO_3$:Eu^{2+}, Mn^{2+} [25], $Ca_3Al_2Si_2O_8Cl_4$:Eu^{2+}, Mn^{2+} [26], and so on.

McKeag and his coworkers reported the emission spectra of Ce^{3+}, Mn^{2+}-codoped barium strontium lithium silicate (BSLS) [27,28], however, no further research about its luminescent properties was made. In this paper, a series of BSLS:Ce^{3+}, Mn^{2+} phosphors was synthesized by solid-state reactions and the photoluminescence (PL) properties were investigated in detail. These phosphors exhibit broad and strong red emission under NUV excitation. The red emission wavelength of Mn^{2+} can be adjusted by

* Corresponding author. Tel.: +86 20 84112830; fax: +86 20 84112245.
E-mail address: cesgml@mail.sysu.edu.cn (M. Gong).

0925-8388/$ – see front matter.
doi:10.1016/j.jallcom.2010.11.139

Table 1
The mole ratio and weight of raw materials for BSLS:Ce^{3+}, Mn^{2+} (Ba = 65, Sr = 10) phosphor.

Raw materials	Molar ratio	Weight (g)
$BaCO_3$	65	0.6413
$SrCO_3$	10	0.0738
SiO_2	50	0.1500
Li_2CO_3	10	0.0370
CeO_2	10	0.0850
$MnCO_3$	5	0.0290
NH_4Cl (flux)	10	0.0267

changing the Ba^{2+}/Sr^{2+} ratio, which is explained by the change of crystal field. The composition-optimized phosphor, BSLS:0.10Ce^{3+}, 0.05Mn^{2+} (Ba = 65), shows the strongest red emission and the best thermal stability.

2. Experimental

The BSLS:Ce^{3+}, Mn^{2+} phosphors were prepared by solid-state reaction. The mole ratio and weight of raw materials $BaCO_3$ (A. R.), $SrCO_3$ (A. R.), Li_2CO_3 (A. R.), SiO_2 (A. R.), $MnCO_3$ (A. R.) and CeO_2 (99.99%) for Ba = 65, Sr = 10 sample are shown in Table 1. The mole percentage of $BaCO_3$, $SrCO_3$ and $MnCO_3$ varies (Ba = 75–∼0; Sr = 0–∼75; Mn = 0–∼11), while those of other raw materials remain constant. They were thoroughly mixed by grinding, then sintered at 900 °C in a reducing atmosphere (N_2:H_2 = 90:10) for 3 h.

X-ray powder diffraction (XRD) patterns of the products were recorded on a Rigaku D/max-IIIA diffractometer with Cu K_α radiation (λ = 1.5403 Å). Photoluminescent excitation and emission spectra, lifetime measurement, as well as temperature-dependent PL spectra of all the phosphors were recorded on an EDINBURGH FLS920 Combined Fluorescence Lifetime & Steady State Spectrometer and a 450 W xenon lamp was used as the excitation source.

3. Results and discussion

3.1. XRD patterns

According to the molar ratio of starting materials, the complete chemical formula for BSLS should be $(Ba_{1.8-x-y-z})(Sr_x)(Li_2)_{0.2}SiO_4$:$yCe^{3+}$, zMn^{2+}, a modification of Ba_2SiO_4. However, the XRD patterns of this product have no peaks matching Ba_2SiO_4, but seem to be a new phase that has not been reported before. As the real formulas of these phosphors remain unknown, we named them by its Ba and Sr molar ratio, such as BSLS:0.10Ce^{3+}, 0.05Mn^{2+} (Ba = 65, Sr = 10). XRD data for the barium strontium lithium silicate compounds in Fig. 1 demonstrates that

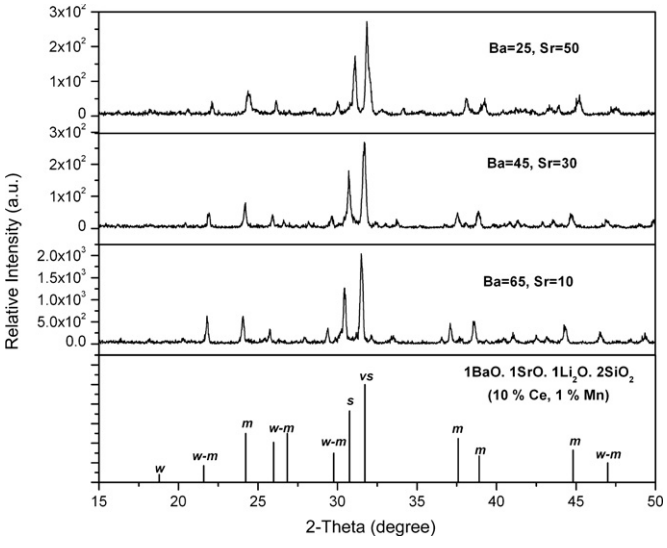

Fig. 1. XRD patterns of BSLS:Ce^{3+}, Mn^{2+} samples (Ba = 65, 45, 25). The bottom represents the XRD pattern based on the reported data [12].

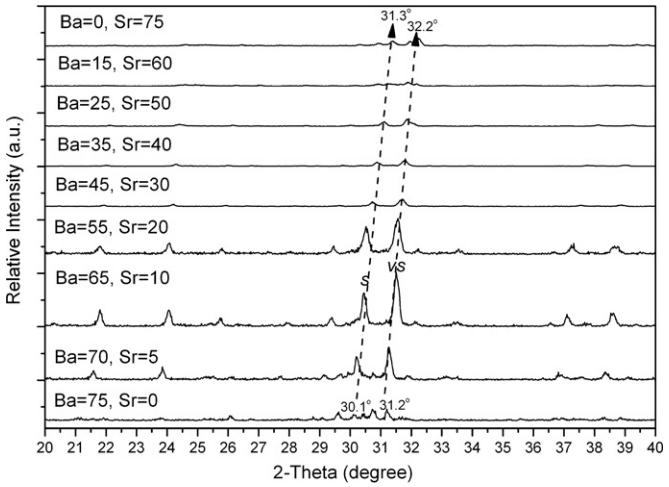

Fig. 2. XRD peak shifting of BSLS:Ce^{3+}, Mn^{2+} phosphors with different Ba:Sr ratios.

a solid solution series is formed by varying the barium/strontium ratio. XRD patterns of the samples with a Ba to Sr ratio of 65 to 10, 45 to 30 and 25 to 50 have the similar profiles with the X-ray diffraction data reported by Mckeag and Steward [27], suggesting that the crystal structure is consisted with the reported sample, and maintains basically unchanged along with the replacement of barium by strontium, except for the different diffraction intensities (see Fig. 1 left tick labels) and the slight right-shifts of diffraction peaks.

Fig. 2 is the partial enlargement of XRD patterns of Ce^{3+}, Mn^{2+} co-doped BSLS phosphors with different Ba:Sr ratios. The 2-theta value of peak *s* increases from 30.1° to 31.3°, and that of peak *vs* rises from 31.2° to 32.2° when barium is generally substituted by strontium. In the similar crystal structure, substituting the larger cation with the smaller one will make crystal cell shrink. According to Bragg equation $2d^* \sin\theta = n\lambda$, the shrinkage of cell volume will lead to the increase of 2-theta value. That is the reason why the 2-theta value shifts right when Ba (r = 135 pm) is generally replaced by Sr (r = 100 pm). It was observed that the crystallinity of the phosphors first increases with strontium-substation, and rises to a maximum for a sample with Ba to Sr ratio of 65 to 10, then generally decreases until barium is completely substituted by strontium. The change in the phosphor crystallinity will affect the emission intensity, which is proven by the following luminescent measurement.

3.2. Photo-luminescent properties

The ground configuration and the excited configuration of Ce^{3+} is $4f^1$ and $5d^1$, respectively. Since the $4f$–$5d$ transition is parity allowed and spin selection is not appropriate, the emission transition is a fully allowed one. Usually Ce^{3+} ion shows broad excitation and emission bands. Fig. 3 demonstrates the PL and PLE spectra of BSLS:0.10Ce^{3+} with a Ba molar ratio of 75 and no Sr substitution. The PLE spectrum shows a broad absorption band from 300 nm to 420 nm, with several peaks located at 253, 287 and 340 nm. Excited by 340 nm-light, the sample exhibits an obvious asymmetric violet-blue emission band around 421 nm, which is ascribed to the $5d^1 \rightarrow 4f^1$ transition of Ce^{3+}.

Since the transitions of Mn^{2+} are $d \rightarrow d$ spin and parity forbidden according to the spin selection rule, the emission and excitation intensities are very weak under UV excitation. The PLE spectrum of BSLS:0.05Mn^{2+} sample (Fig. 3 orange line, left) consists of several peaks centering at 350, 365, 405, 421 and 500 nm, corresponding to the well-known transitions of Mn^{2+} from ground level $^6A_1$ (^6S) to ^4E (^4D), $^4T_2$ (^4D), [$^4A_1$ (^4G), ^4E (^4G)], $^4T_2$ (^4G) and $^4T_1$ (^4G) levels. An

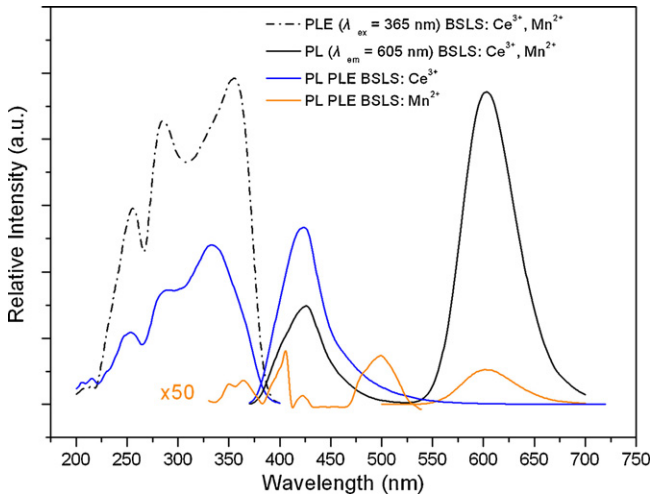

Fig. 3. PL and PLE spectra of BSLS:0.10Ce^{3+}, 0.05Mn^{2+}, BSLS:0.10Ce^{3+} and BSLS:0.05Mn^{2+} (Ba = 75) phosphor.

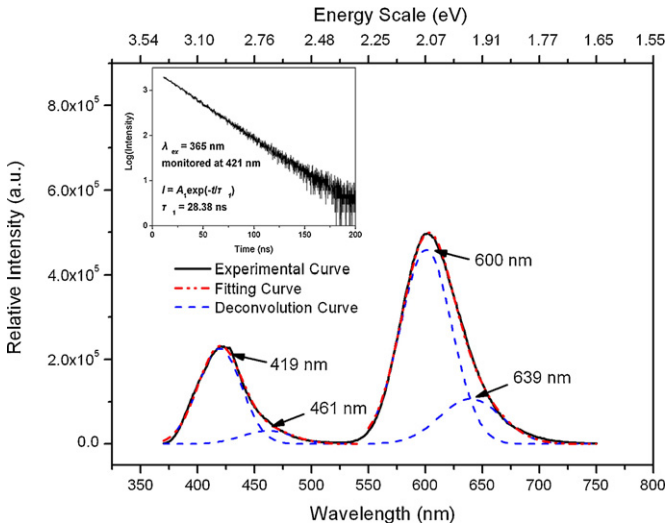

Fig. 4. Experimental spectrum (solid line), fitting curve (red dash line), and deconvolution Gaussian curve (blue dash line) of BSLS:0.10Ce^{3+}, 0.05Mn^{2+} (Ba = 75). The inset shows Ce^{3+} emission decay in BSLS:0.10Ce^{3+}. (For interpretation of the references to color in this figure caption, the reader is referred to the web version of the article.)

orange-reddish emission peak centering at 605 nm appears in the PL spectrum, which arises from the transition $^4T_1 \rightarrow {}^6A_1$ of Mn^{2+}.

The PLE spectrum of BSLS:0.10Ce^{3+} phosphor shows a broad excitation band with several peaks at 253, 287 and 340 nm while it gives a broad violent-blue emission under near UV excitation (Fig. 3). PLE spectrum of the BSLS:0.10Ce^{3+}, 0.05Mn^{2+} (Ba = 75) is similar to that for the single Ce^{3+}-doped sample except for much higher intensity and some red shift to 256, 285 and 365 nm. However, compared with the PL spectrum of the single Ce^{3+}-doped sample, besides the violent-blue emission band with decreased intensity from Ce^{3+}, a broad and strong orange-reddish band appears, which is due to Mn^{2+} sensitized emission and its intensity is much stronger than that of the single Mn^{2+}-doped sample. The result indicates that efficient energy transfer from Ce^{3+} to Mn^{2+} happens in the Ce^{3+}–Mn^{2+} co-doped sample. This phenomenon is easy to understand since the Ce^{3+} emission covers some Mn^{2+} excitation band and the excitation spectrum of BSLS:Ce^{3+}, Mn^{2+} monitoring the Mn^{2+}-derived emission has similar profile with the excitation bands of BSLS:Ce^{3+}.

The Ce^{3+} emission band seems to be asymmetric on the long wavelength region, which indicates the existence of different luminescent peaks. Based on the Gaussian fitting, the Ce^{3+} emission band in the Ce^{3+}–Mn^{2+} co-doped sample consists of two peaks at 419 and 461 nm (see Fig. 4). The energy difference was about 2174 cm^{-1}, which agrees well with the theoretical value of spin–orbit splitting between the 4*f* ground state $^2F_{5/2}$ and $^2F_{7/2}$ (about 2200 cm^{-1}), indicates Ce^{3+} ions locate at one kind of crystallographic site. The inset shows the decay lifetime of BSLS:0.10Ce^{3+} excited at 365 nm, monitoring at 421 nm. The results again proved that Ce^{3+} occupied one site since it was best fitted with single decay constant, τ_1 = 28.38 ns.

Tetrahedrally coordinated Mn^{2+} (weak crystal-field) usually gives a green emission while octahedrally coordinated Mn^{2+} (strong crystal-field) gives an orange to red emission [29]. The Mn^{2+} emission in the red spectral region indicates the strong crystalline field on the Mn^{2+} site in the BSLS host. We speculate that there is one type of occupied site for Ce^{3+} ions in the lattice and it also is true for the Mn^{2+} ions, However, the asymmetric red emission band of Mn^{2+} was deconvoluted into two peaks centering at 600 and 639 nm (Fig. 4, blue dashed lines).

As indicated above, there is only a single crystallographic site on which Mn^{2+} will incorporate. As a consequence, it is expected that there is only one crystallographic site for Mn^{2+}, which would result in a single narrow symmetric emission band. However, two over-lapping emission bands have been observed in the emission spectra. Possible explanation for the appearance of two emission bands is the formation of paired Mn^{2+} centers besides the Mn^{2+}

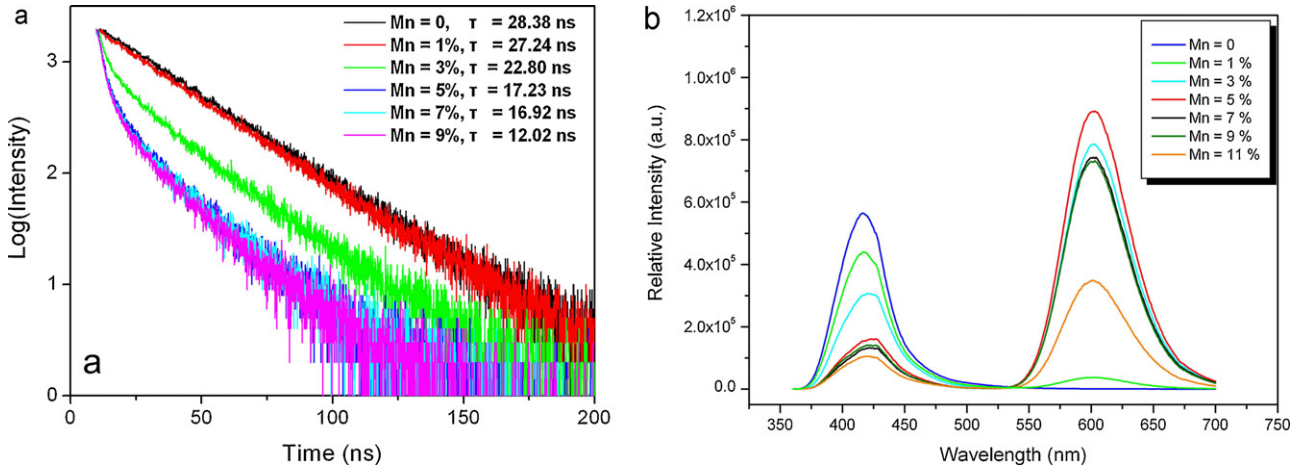

Fig. 5. Decay curves of Ce^{3+} emission (a) and the emission spectra (b) of BSLS:0.10Ce^{3+}, *x*Mn^{2+} (Ba = 75, *x* = 0–0.11) phosphors (λ_{ex} = 365 nm).

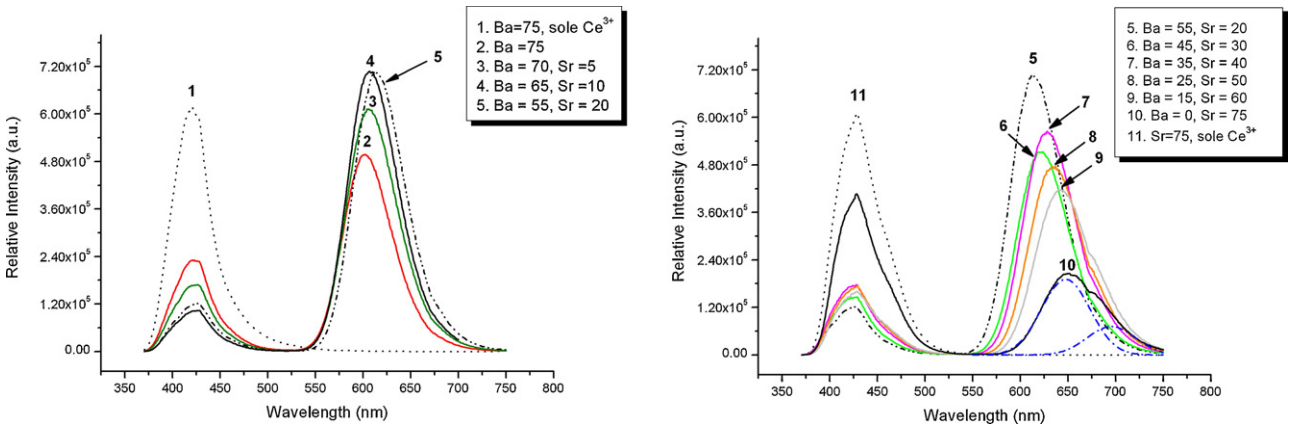

Fig. 6. PL spectra of Ce^{3+}, Mn^{2+} co-doped and Ce^{3+} sole-doped BSLS phosphors with different Ba:Sr ratios (λ_{ex} = 365 nm).

center on the regular site in BSLS. In fact, such paired Mn^{2+} centers have been observed in a lot of Mn^{2+}-doped phosphors, such as Zn_2SiO_4:Mn^{2+} [30] and MS:Mn^{2+}(M = Mg, Ca, Sr) [31–33]. The tendency of two different emission profiles for Mn^{2+} emission becomes more and more obvious as the Sr^{2+} content increases (see Fig. 6, sample 10). We speculate the reason is that Sr^{2+} codoping could accelerate the formation of paired Mn^{2+} centers.

The decay curves of BSLS:0.10Ce^{3+}, $x$$Mn^{2+}$ phosphors excited at 365 nm and monitored at 421 nm are shown in Fig. 5a. Ce^{3+} emission decay of BSLS:Ce^{3+}, Mn^{2+} sample becomes more and more non-exponential with rising Mn^{2+} content. The decay constant τ reduced monotonically from 28.38 to 12.02 ns as x increases from 0 to 0.09, which is a good evidence for $Ce^{3+} \rightarrow Mn^{2+}$ energy transfer.

It is considered that the energy transfer proceeds by Förster resonance energy transfer (FRET) mechanism [34,35] (energy transfer via electric multipole–multipole interaction) for the following two reasons: (i) BSLS:Ce^{3+}, Mn^{2+} sample exhibited no clear excitation band at Ce^{3+} emission wavelengths and (ii) peak profile of Ce^{3+} emission does not change before and after Mn^{2+}-addition. Probably dipole–quadruple interaction plays an important role in the FRET process, as suggested for Eu^{2+}, Mn^{2+}-doped BAM [36].

The PL spectra of BSLS:0.10Ce^{3+}, $x$$Mn^{2+}$ (Ba = 75, x = 0–~0.11) under excitation of 365 nm are displayed in Fig. 5b. The intensity of Ce^{3+} blue emission decreases with an increasing doped Mn^{2+} concentration. In contrast, the PL intensity of Mn^{2+} emission increases until the Mn^{2+} concentration quenching happens with a content of 0.05. The observed variations in the emission intensities of Ce^{3+} and Mn^{2+} strongly indicate the efficient energy transfer from Ce^{3+} to Mn^{2+}. As BSLS:0.10Ce^{3+}, 0.05Mn^{2+} (Ba = 75) exhibits the strong emission intensity in this series, this doped Ce^{3+} and Mn^{2+} concentrations were chosen for further investigation.

3.3. Effect of Ba:Sr ratio on emission spectra

The emission spectra of Ce^{3+}, Mn^{2+} co-doped and Ce^{3+} sole-doped BSLS phosphors with different Ba:Sr ratios (λ_{ex} = 365 nm) are presented in Fig. 6. As seen in Fig. 6, the Mn^{2+} emission peak shows red-shift from 605 nm for Ba = 75 sample, to 650 nm for Sr = 75 sample, while Ce^{3+} emission peak shifts from 421 nm to 430 nm. The Mn^{2+} ion has an emission which consists of a broad band, the position of which depends strongly on the host lattice due to the dependence on crystal field. Thus, the choice of the host is a critical parameter for determining the optical properties of Mn^{2+} [37]. In this regard, the crystal field around Mn^{2+} has been suggested as obeying [38]:

$$\Delta = Dq = \frac{ze^2r^4}{6R^5} \quad (2)$$

where Dq ($=\Delta$) is a measurement of the crystal-field strength, z is the charge or valance of the anion, e is the charge of an electron, r is the radius of the d wave function, and R is the distance between the central ion and its ligands. For the BSLS host, the crystal volume shrinks with the replacement of barium by strontium, which is confirmed by XRD data. Since the strong dependence of Dq on R, a stronger crystal field can be expected with increasing Sr^{2+} replacement.

It is well known that Tanabe–Sugano diagrams explain very well the characteristics of optical spectra due to the intra-3d shell transition of transition metal ions in host lattices. According to the diagram for the $3d^5$ electron configuration of Mn^{2+}, the energies of the $^4E(^4G)$, $^4A_1(4G)$ states and $^4E(^4D)$ state relative to the $^6A_1(^6S)$ ground state are insensitive to the crystal-field strength Dq [39]. On the other hand, the Tanabe–Sugano diagram predicts

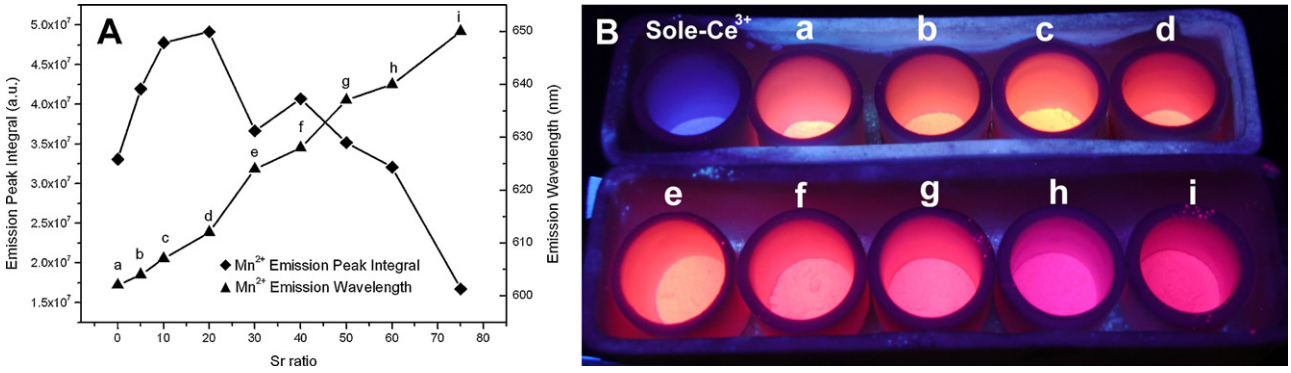

Fig. 7. The Mn^{2+} emission peak integral and emission wavelength as a function of Sr^{2+} ratio (A), and photo of Ce^{3+}, Mn^{2+} co-doped and Ce^{3+} sole-doped BSLS phosphors with different Ba:Sr ratios under 365 nm radiation (B).

that the energy separations between the $^4T_1(^4G)$ and $^4T_2(^4G)$ states and the $^6A_1(^6S)$ ground state are very sensitive to the crystal-field strength *Dq* and decreases with increase of crystal field strength. It is well known that the emission bands of Mn^{2+} originate from the $^4T_1(^4G)$–$^6A_1(^6S)$ transition. Therefore, the position of the emission bands of Mn^{2+}-doped phosphors is largely determined by the crystal field strength of Mn^{2+} in the host lattice [40].

For the isostructural compounds of BSLS, the metal–ligand distances are smaller when Ba^{2+} was replaced by Sr^{2+} because Ba^{2+} is larger than Sr^{2+}. As a consequence, the crystal field strength becomes stronger for Mn^{2+} when Ba^{2+} is replaced by Sr^{2+} in BSLS host lattice, which results in the decrease of energy separation between the $^4T_1(^4G)$ states and the $^6A_1(^6S)$ ground state, and the longer wavelength emission band of Mn^{2+} in BSLS host lattice. Similar emission redshift and explanation can be found in Mn^{2+}-activated $M_2Si_5N_8$ (M = Ca, Sr, Ba) [40] and $MSiN_2$ (M = Mg, Zn) [41].

Fig. 7A shows the Mn^{2+} emission peak integral and emission wavelength as a function of Ba^{2+} content. As Ba amount decreases from 75 to 0, the emission intensity first rises to a maximum at Ba = 65, then generally declines. The change of emission intensity has the same tendency with that of crystalline, which is demonstrated through the peak intensities in Section 3.1. We could not exclude the possibility that red emission comes from other phases than the barium strontium lithium silicate when the sample's crystallinity is low. But the sample with high crystallinity has the similar emission spectra profile with low crystallinity one, indicated that even in the situation of low crystallinity, red emission mainly comes from the barium strontium lithium silicate phase. Photo of BSLS phosphors with different Ba:Sr ratios under 365 nm radiation is shown in Fig. 7B.

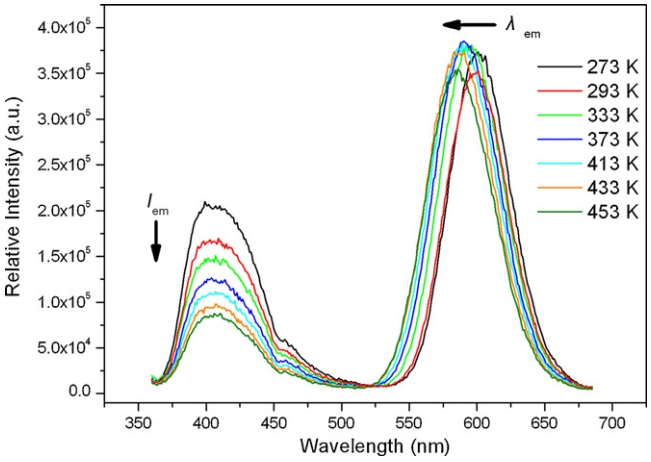

Fig. 8. The emission spectra measured at different temperatures of BSLS:0.10Ce^{3+}, 0.05Mn^{2+} (Ba = 75) phosphors (λ_{ex} = 365 nm).

3.4. Thermal stability

Fig. 8 shows the temperature dependent emission spectra of BSLS:0.10Ce^{3+}, 0.05Mn^{2+} (Ba = 75) phosphor from room temperature to 180 °C. The relative peak intensities of Ce^{3+} decreased generally with temperature, and it reached 50% of the initial value

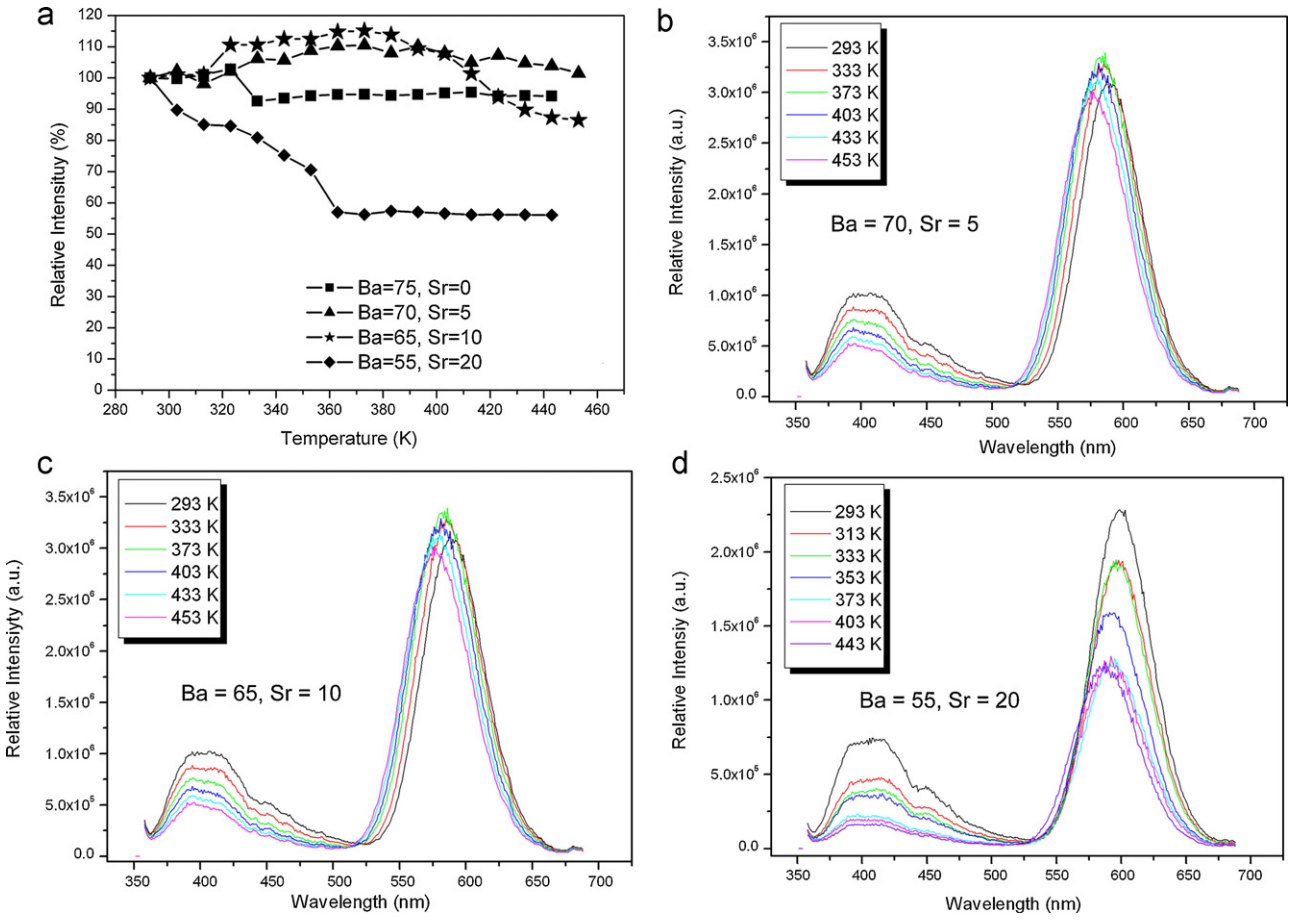

Fig. 9. Temperature-dependent relative emission intensities of Mn^{2+} (a) for BSLS:Ce^{3+}, Mn^{2+} phosphors (Ba = 75, 70, 65, 55), and emission spectra measured at different temperatures of BSLS:0.10Ce^{3+}, 0.05Mn^{2+} (Ba = 70, 65, 55) phosphors (λ_{ex} = 365 nm).

at 140 °C and 40% at 180 °C, respectively. The thermal stability of Mn^{2+} emission is higher than those of Ce^{3+} emission. The Mn^{2+} emission intensity slightly declined to 94% at 180 °C.

As seen in Fig. 8, the Mn^{2+} emission wavelength blue-shifts with increasing temperature. The peak positions at 273 K and 443 K are 605 nm and 587 nm, respectively. It is considered that thermal active phonon-assisted excitation from lower energy sublevel to higher energy sublevel in excited states occurs [42,43]. Elevated temperature causes electrons at lower energy level to jump to higher energy levels by phonon assistance whereas the nonradiative transitions from excited states to ground states are prevented. At higher temperature, more electrons are populated at higher-energy excited sublevel, but the nonradiative transitions through the crossing point between the excited state and the ground state in configurational coordinate diagram are decreased. The height of higher-energy emission peak is increased, and that of lower-energy emission peak is decreased. As a result, the blue-shift behavior is observed with increasing temperature [44].

Fig. 9 shows the temperature dependent relative emission intensity of BSLS:0.10Ce^{3+}, 0.05Mn^{2+} phosphors (Ba = 75, 70, 65, 55) from room temperature to 180 °C. In Fig. 9a, we set Mn^{2+} emission intensity at 293 K as 100% for different samples, respectively and compare it with other emission intensities at higher temperature. The relative peak intensities of Ce^{3+} (excited at 365 nm) decreased generally with temperature, and stronger thermal quench appears when the ratio of Ba^{2+} drops. It reached 53%, 50%, 41% and 22% of initial value at 180 °C for Ba = 75, 70, 65, 55 sample, respectively (see Fig. 9b–d). The thermal stabilities of Mn^{2+} emission are higher than those of Ce^{3+} emission. The Mn^{2+} emission intensity (Ba = 75) slightly declines to 94% at 180 °C, while those of Ba = 70 and 65 sample remains almost the same as the initial value even at 180 °C, which demonstrates that certain Sr^{2+}-codoped can enhance the thermal stability of Mn^{2+} emission. But when the ratio of Sr rises to 20%, both thermal stabilities of Ce^{3+} and Mn^{2+} emission become worse than the original Ba = 75 sample.

The decrease in emission intensity with increasing temperature is due to the temperature dependence of the electron–phonon interaction in both the ground state and excited states of the luminescence center. This nonradiative transition probability by thermal activation is strongly dependent on temperature, resulting in the decrease of the emission intensity [45]. Comparatively, the thermal quenching temperature of Mn^{2+} was higher than that of Ce^{3+}, indicating a weaker electron–phonon interaction or higher thermal activation energy in the host [19].

In a high-pressure lamp the discharge emits strong line at 365 nm and considerable amount of blue and green lights. And by changing the indium content in $Ga_{1-x}In_xN$, LED emission can be tuned to 360–370 nm, white light can be produced by long-wave UV excitation of a blend of phosphors. Therefore, an ideal red phosphor for both applications is required to absorb long wavelength UV radiation, emit strong red light and have excellent thermal stability. Because BSLS:Ce^{3+}, Mn^{2+} (Ba = 65) phosphor has the strongest excitation and emission intensity and best thermal stability, is suitable for NUV LED or high pressure Hg vapor (HPMV) lamps.

4. Conclusions

(1) A series of red emitting Ce^{3+}, Mn^{2+}-codoped barium strontium lithium silicate (BSLS) phosphors was synthesized by a high-temperature solid-state reaction. The BSLS:Ce^{3+}, Mn^{2+} phosphor showed two emission bands under 365 nm excitation, one observed at 421 nm was attributed to Ce^{3+} emission, and another found at red region was assigned to Mn^{2+} emission due to efficient $Ce^{3+} \rightarrow Mn^{2+}$ energy transfer.

(2) The Mn^{2+} emission peak shifts right along with the replacement of barium by strontium, which is due to stronger crystal field. The Mn^{2+} emission intensity and thermal stability are affected by strontium substitution. BSLS:0.10Ce^{3+}, 0.05Mn^{2+} with a Ba molar ratio of 65 shows the strongest emission intensity and best thermal stability, and therefore is suitable for application as red component in NUV LED or high pressure Hg vapor (HPMV) lamps.

Acknowledgement

This work was funded by a research grant from the Natural Science Foundation of China (no. 50672136).

References

[1] S. Lee, S. Seo, J. Electrochem. Soc. 149 (2002) J85–J88.
[2] X.G. Zhang, X.P. Tang, J.L. Zhang, H.H. Wang, J.X. Shi, M.L. Gong, Powder. Technol. 204 (2010) 263–267.
[3] R.J. Xie, N. Hirosaki, Sci. Technol. Adv. Mater. 8 (2007) 588–600.
[4] Z. Wang, H. Liang, L. Zhou, J. Wang, M. Gong, Q. Su, J. Lumin. 128 (2008) 147–154.
[5] X.F. Qu, L.X. Cao, W. Liu, G. Su, C. Xu, P.P. Wang, J. Alloys Compd. 494 (2010) 196–198.
[6] I.M. Nagpure, K.N. Shinde, V. Kumar, O.M. Ntwaeaborwa, S.J. Dhoble, H.C. Swart, J. Alloys Compd. 492 (2010) 384–388.
[7] X.M. Zhang, H.P. Zeng, Q. Su, J. Alloys Compd. 441 (2007) 259–262.
[8] Y.H. Liu, Z.Y. Mao, W.H. Yu, Q.F. Liu, D.J. Wang, J. Alloys Compd. 493 (2010) 406–409.
[9] S. Abe, K. Uematsu, K. Toda, M. Sato, J. Alloys Compd. 408–412 (2006) 911–914.
[10] T. Aitasalo, A. Hietikko, D. Hreniak, J. Holsa, M. Lastusaari, J. Niittykoski, W. Strek, J. Alloys Compd. 451 (2008) 229–231.
[11] L. Lin, C.S. Shi, Z.F. Wang, W.P. Zhang, M. Yin, J. Alloys Compd. 446 (2008) 546–550.
[12] T.G. Kim, Y.S. Kim, S.J. Im, J. Electrochem. Soc. 156 (2009) J203–J207.
[13] Y.K. Kim, S. Choi, H.K. Jung, J. Lumin. 130 (2010) 60–64.
[14] P.L. Li, Z.J. Wang, Z.P. Yang, Q.L. Guo, J. Electrochem. Soc. 157 (2010) H504–H509.
[15] C.H. Huang, W.R. Liu, T.M. Chen, J. Phys. Chem. C 114 (2010) 18698–18701.
[16] Z.P. Yang, S.Y. Ma, H.W. Yu, F.H. Wang, X. Ma, Y.F. Liu, P.L. Li, J. Alloys Compd. 509 (2011) 76–79.
[17] N.S. Choi, K.W. Park, B.W. Park, X.M. Zhang, J.S. Kim, P. Kung, S.M. Kim, J. Lumin. 130 (2010) 560–566.
[18] X.M. Zhang, H.J. Seo, Physica B 405 (2010) 2436–2439.
[19] W.R. Liu, Y.C. Chiu, Y.T. Yeh, S.M. Jang, T.M. Chen, J. Electrochem. Soc. 156 (2009) J165–J169.
[20] C.H. Huang, T.W. Kuo, T.M. Chen, ACS Appl. Mater. Interfaces 2 (2010) 1395–1399.
[21] X.G. Zhang, J.L. Zhang, R. Wang, M.L. Gong, J. Am. Ceram. Soc. 93 (2010) 1368–1371.
[22] S.S. Yao, Y.Y. Li, L.H. Xue, Y.W. Yan, J. Alloys Compd. 491 (2010) 264–267.
[23] Y. Umetsu, S. Okamoto, H. Yamamoto, J. Electrochem. Soc. 155 (2008) J193–J197.
[24] W.J. Xie, J.Y. Tang, L.Y. Hao, X. Xu, Opt. Mater. 32 (2009) 274–276.
[25] S. Ye, X.M. Wang, X.P. Jing, J. Electrochem. Soc. 155 (2008) J143–J153.
[26] Z.G. Xia, P. Du, L.B. Liao, G.W. Li, S. Jin, Curr. Appl. Phys. 10 (2010) 1087–1091.
[27] A.H. McKeag, E.C. Steward, Br. J. Appl. Phys. 4 (1955) 26–31.
[28] A.H. McKeag, J. Electrochem. Soc. 105 (1958) 78–81.
[29] G. Blasse, B.C. Grabmaier, Luminescent Materials, Springer-Verlag, Berlin, 1994.
[30] C. Barthou, J. Benoit, P. Benalloul, A. Morell, J. Electrochem. Soc. 141 (1994) 524–528.
[31] S. Asano, N. Yamashita, Y. Nako, Y. Matsushima, Phys. Stat. Solidi B 108 (1981) 229–239.
[32] N. Yamashita, S. Maekawa, K. Nakamura, J. Appl. Phys. Jpn. 29 (1990) 1729–1732.
[33] I. Matsuyama, N. Yamashita, K. Nakamurar, J. Phys. Soc. Jpn. 58 (1989) 741–751.
[34] S. Kamiya, H. Mizuno, Phosphor Handbook, CRC Press, Boca Raton, FL, 1999.
[35] Y. Yonesaki, T. Takei, et al., J. Solid State Chem. 183 (2010) 1303–1308.
[36] C.H. Park, S.T. Hong, D.A. Kezsler, J. Solid State Chem. 182 (2009) 496–501.
[37] Z.P. Ci, Y.H. Wang, J. Electrochem. Soc. 159 (2009) J267–J272.
[38] P.D. Rack, P.H. Holloway, Mater. Sci. Eng. B 21 (1998) 171.
[39] J.S. Griffith, The Theory of Transition-Metal Ions, Cambridge University Press, Cambridge, 1961.
[40] C.J. Duan, W.M. Otten, A.C.A. Delsing, H.T. Hintzen, J. Solid State Chem. 181 (2008) 751–757.
[41] C.J. Duan, A.C.A. Delsing, H.T. Hintzen, J. Lumin. 129 (2009) 645–649.
[42] D. Hsu, J.L. Skinner, J. Chem. Phys. 81 (1984) 1604–1613.
[43] D. Hsu, J.L. Skinner, J. Chem. Phys. 81 (1984) 5471–5479.
[44] J.S. Kim, Y.H. Park, J.C. Choi, H.L. Park, Electrochem. Solid State 8 (2005) H65–H67.
[45] W.J. Ding, J. Wang, Z.M. Liu, M. Zhang, Q. Su, J.K. Tang, J. Electrochem. Soc. 155 (2008) J122–J127.